Organized AlN Nanowire Arrays by Hybrid Approach of Top-Down Processing and MOVPE Overgrowth for Deep UV Emission Devices

Lucie Valera, Lucas Jaloustre, Valérie Reita, Saron R.S. de Mello, Edith Bellet-Amalric, Camille Petit-Étienne, Erwine Pargon, Gwenolé Jacopin, Christophe Durand

▶ **To cite this version:**

Lucie Valera, Lucas Jaloustre, Valérie Reita, Saron R.S. de Mello, Edith Bellet-Amalric, et al.. Organized AlN Nanowire Arrays by Hybrid Approach of Top-Down Processing and MOVPE Overgrowth for Deep UV Emission Devices. ACS Applied Nano Materials, 2024, 7 (9), pp.10338-10349. 10.1021/acsanm.4c00814 . hal-04568259

HAL Id: hal-04568259
https://hal.science/hal-04568259v1

Submitted on 9 Oct 2024

HAL is a multi-disciplinary open access archive for the deposit and dissemination of scientific research documents, whether they are published or not. The documents may come from teaching and research institutions in France or abroad, or from public or private research centers.

L'archive ouverte pluridisciplinaire **HAL**, est destinée au dépôt et à la diffusion de documents scientifiques de niveau recherche, publiés ou non, émanant des établissements d'enseignement et de recherche français ou étrangers, des laboratoires publics ou privés.

Organized AlN Microwire Arrays by Hybrid Approach of Top-Down Processing and MOVPE Overgrowth for deep UV emission.

Lucie Valera[1,2], Lucas Jaloustre[3], Valérie Reita[2], Saron R.S. De Mello[2,3], Camille Petit-Étienne[3], Erwine Pargon[3], Gwénolé Jacopin[2], Christophe Durand[1]

[1] Univ. Grenoble Alpes, Grenoble-INP, CEA, IRIG, PHELIQS, NPSC, Grenoble, France

[2] Univ. Grenoble Alpes, CNRS, Grenoble INP, Institut Néel, Grenoble, France

[3] Univ. Grenoble Alpes, CNRS, CEA/LETI-Minatec, Grenoble INP, Institute of Engineering and Management University Grenoble Alpes, LTM, Grenoble, France

Keywords: AlN, microwires, top-down etching, MOVPE

Abstract:

The fabrication of organized AlN pillars with well faceted m-sidewalls is demonstrated, exhibiting a narrow near band edge emission that confirms the high-quality of the AlN materials. In the first step, a top down approach combining plasma etching process and subsequent wet KOH allows to fabricate strain-free AlN pillars with various density and diameters as small as 250 nm with m–oriented facets. In a second step, optimized overgrowth by MOVPE is performed to recover m-oriented hexagonal facets. A growth model is proposed to fit the evolution of the AlN lateral growth rate as a function of the spacing and diameter of the AlN pillars, highlighting two main contributions : diffusion from the substrate and direct vapor phase contribution. Cathodoluminescence measurements at 5 K and 300 K reveal that the overgrown AlN layer exibits intense AlN near-band edge emission, confirming that this hybrid approach is suitable to create high quality m-oriented AlN template.

Introduction

The demand for performant UV-C (< 280 nm) LEDs has raised in recent years, especially due to their bactericidal or virucidal applications.[1–5] However, despite constant efforts in the development of deep-UV LEDs, its efficiency still suffers from the following recurrent issues: poor doping of AlGaN materials,[6–8] high density of defects in the AlGaN layers[9] and poor extraction of the emitted light.[10] In this context, innovative solutions are explored to increase the efficiency of deep UV-LEDs, leading to the reconsideration of the first technological building block of the LED: the template. The template is traditionally composed of a c-oriented AlN layer grown on sapphire substrate. Unfortunately, the high lattice mismatch between AlN and sapphire (13%) leads to a high density of threading dislocations, which will mostly propagate into the active region.[11] Thus, the use of nanostructured templates is an attractive alternative to regular planar templates, due to the reduced defect density[12–14] and the improved light extraction expected in nanostructured LED.[15–17] In this context, nano/microwire-based templates or fin-based templates[18] are particularly interesting due to their exposed non-polar facets. This provides non-polar planes for the growth of the active region, allowing thicker quantum wells by suppressing the quantum confined Stark effect (QCSE) in the active region. For now, the use of GaN nano/microwires as template have been reported, leading to the demonstration of UV-A and UV-B wire-based LEDs.[19–21] Nevertheless, the large lattice mismatch between the GaN wire and the AlGaN layers in UV LED structure leads to drastic strain issues involving crack formation.[22] In addition, GaN is not UV-C transparent, which makes GaN wires definitely not suitable for UV-C LED design. The use of AlN nano/micro-wires array would overcome the disadvantages of the GaN ones mentioned above. Unfortunately, the MOVPE growth of bottom-up AlN nano/micro-wire arrays is very challenging and a top-down process is highly preferred, even if the AlN microwire arrays

already reported in the literature suffer from poor optical properties.[23] In this work, we present the fabrication of organized AlN nanopillar array using a hybrid approach combining top-down processing and MOVPE overgrowth. First, top-down fabrication of AlN array using both dry and wet etching is presented. Then, the MOVPE overgrowth conditions to obtain micro-wires with well-defined facets as well as growth mechanisms are investigated. The optical properties of original AlN planar template, AlN pillars after the top-down process and AlN wires after the MOVPE overgrowth are investigated by cathodoluminescence (CL) measurements.

Results and Discussion

1. Focus on the 1st process step: top-down etching

The AlN micro-pillars are fabricated on a commercially available 2-inch wafer using an unintentionally doped Al-polar (0001) 3-µm thick AlN layer grown on a c-sapphire substrate provided by Nanowin company. A 800 nm-thick SiO_2 hard mask (HM) is deposited onto the AlN layer using Plasma Enhanced Chemical Vapor Deposition (PECVD). The structure of the sample is illustrated in **Fig. 1(a)**. Then, the wafer is diced into small coupons measuring 1.1 by 0.7 cm. An electron-sensitive resist (ma-N 2410) with a thickness of 800 nm is spin-coated and patterned using electron beam lithography (EBL). The patterns consist of hexagonal dots, with diameters D (inscribed circle) ranging from 0.25 to 2 µm, using three different densities (spacing S between dots of 2, 5 and 15 µm) (see **Fig. 1(a)**). The hexagonal dots are oriented to match the m-planes of AlN, with a precision of ±1 °.

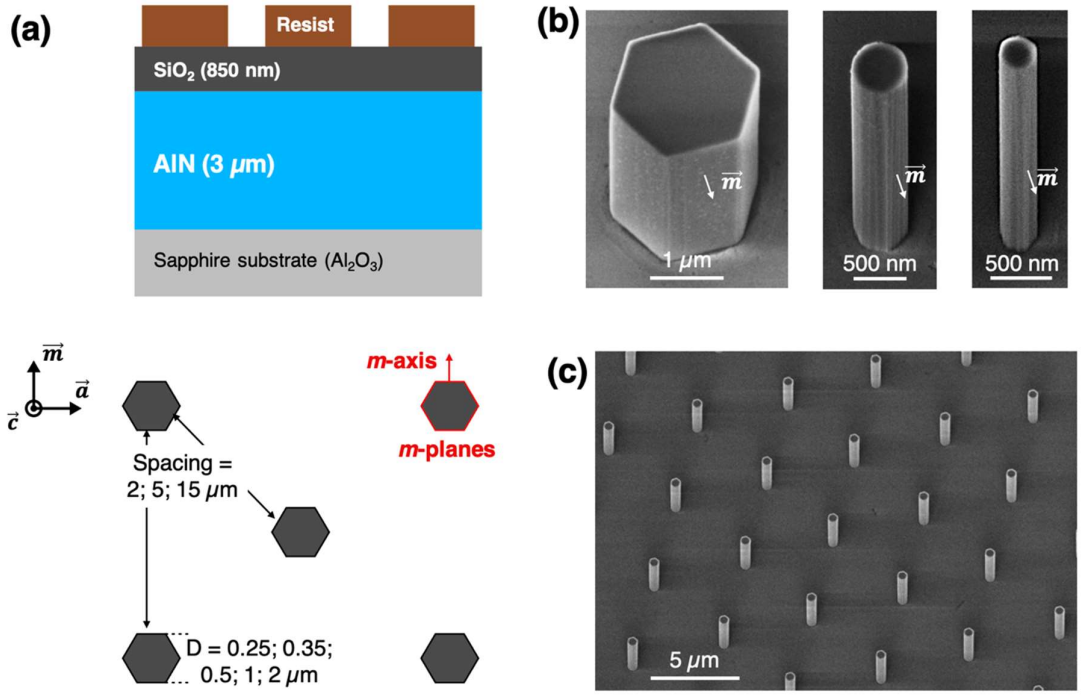

<u>Figure 1:</u> (a) Schematic of the structure before top-down process with the design of the lithography pattern (diameter D varying between 250 nm and 2 µm and spacing S varying between 2 and 15 µm). (b) Tilted SEM images of single AlN wire after the full top-down process for three diameters (2 µm, 500 nm and 250 nm) and (c) a lower magnification SEM image of on specific array: D = 500 nm, S = 5 µm.

The etching experiments are conducted using a Centura 5200 etch platform from Applied Materials, which comprises three plasma reactors.[24,25] For the HM opening step, the AlN samples are thermally glued onto a 200 mm SiO_2 carrier wafer using silicone-free thermal paste (Type 1977-DP) from Techspray, and the HM was etched with an $Ar/C_4F_8/O_2$ plasma in the Magnetically Enhanced Reactive Ion Etching (MERIE) reactor. Subsequently, for both resist stripping and AlN etching steps, the samples are thermally glued on a 200 mm SiN carrier wafer, and the plasma processes are operated in an Inductively Coupled Plasma (ICP) reactor (Decoupled Plasma Source, DPS, from Applied Materials). The resist are stripped using an O_2 plasma, while the AlN layer is etched with a Cl_2 plasma using the following parameters: Cl_2 flow of 190 sccm, source power of 400 W, Pressure of 20 mTorr, and a bias power of 150 W (which corresponds to a direct current voltage on the chuck of -450 V).

The AlN plasma etching is monitored in real-time and stopped at the end of the process using an endpoint system that utilizes interferometry with a Xenon lamp providing wavelengths from 200 to 800 nm. After plasma patterning, the AlN samples are dipped in a KOH solution (5 wt% KOH diluted in H_2O) during 1 hour. Then, the SiO_2 HM is removed with a 50% HF solution during 5 min. The fabrication of *m*-facetted AlN pillars by using a Cl_2 plasma patterning followed by wet KOH, shown in this study, results from previous studies on the fabrication of m-facetted GaN pillars with the same masking strategy.[24,25] The Cl_2 plasma and

wet KOH conditions have been slightly adapted to AlN case. However, similar experimental set up had been used and is fully described in the following reference.[24,25] Moreover, the mechanisms leading to m-faceting with the two step process are also fully explained, the key being to combine a slightly sloped AlN profile after Cl_2 plasma etching with the use of an m-oriented HM during the wet KOH treatment.[25]

Fig. 1(b) shows three SEM pictures after the full top-down process of three single AlN pillars with diameter of 2 µm, 500 nm and 250 nm, respectively (S = 5 µm). Pillars exhibit distinct facets with sharp edges for the 2 µm wire, while rounder edges are observed for the 500 nm and 250 nm wires. **Fig. 1(c)** shows a view-bird SEM picture with a lower magnification of one AlN array (D = 500 nm and S = 5 µm), revealing highly homogeneous wire-to-wire morphology. **Fig.S1** in Supplementary Materials shows additional SEM images of AlN micropillar arrays, highlighting its high homogeneities.

Micro-Raman measurements are performed to compare the strain state of AlN template and AlN pillar arrays after the top-down process. Raman spectra are recorded using an Alpha 500 Witec Raman microscope with 50 X microscope objective. The excitation laser is a 532.12 nm green laser and the incident power on the samples is 4 mW. Resulting Raman spectra of the AlN template and the AlN micro-pillars with diameter of 250 nm, 500 nm and 2 µm are pictured in **Fig. 2**. Multiple modes are noticeable and are identified by referring to the literature[26–29]: 603-628 cm^{-1} attributed to AlN A_1 (TO), 643-670 cm^{-1} coming from AlN E_2 (high), 662-680 cm^{-1} from E_1 (TO), 738-750 cm^{-1} attributed to sapphire and 873-913 cm^{-1} from AlN A_1 (LO). As the frequency of the E_2 (high) mode is sensitive to the strain state in AlN materials, the Raman analysis are focused on this mode.[30–33] The inset in **Fig. 2** shows a zoom on the E_2 (high) mode for all the spectra. The dots represent the experimental data, which are fitted on a lorentzian evolution represented by the full lines. The line widths for the E_2 (high) modes are

between 3.7-4.2 cm^{-1}, suggesting a good crystal quality maintained through the etching process. The lorentzian curves associated to AlN template and AlN pillar array with 250 nm, 500 nm and 2 µm diameter are centered around 662.7, 655.4, 655.3 and 655.5 cm^{-1}, respectfully. For the three diameters of wires considered here, a similar frequency shift of ≈7.3 ± 0.1 cm^{-1} is measured for the AlN pillar array after the top-down process compared to the original AlN template. This observation can be interpreted as the result of strain relaxation mechanisms after the etching process, which is equivalent for the three diameters considered. This observation confirms that the use of nanostructures is an efficient approach to create strain-free templates, as previously observed in the literature.[34] Referring to the literature, the E_2 (high) frequency for relaxed AlN is 655 cm^{-1}, indicating that the wires are almost fully relaxed after the etching process.[31] Moreover, the observed shift corresponds approximately to a strain relaxation of 0.38 % assuming a biaxial strain.[35,36] The lattice mismatch between AlN and sapphire being 13%, the 3 µm-thick AlN template is estimated to be already almost relaxed before any top-down process.

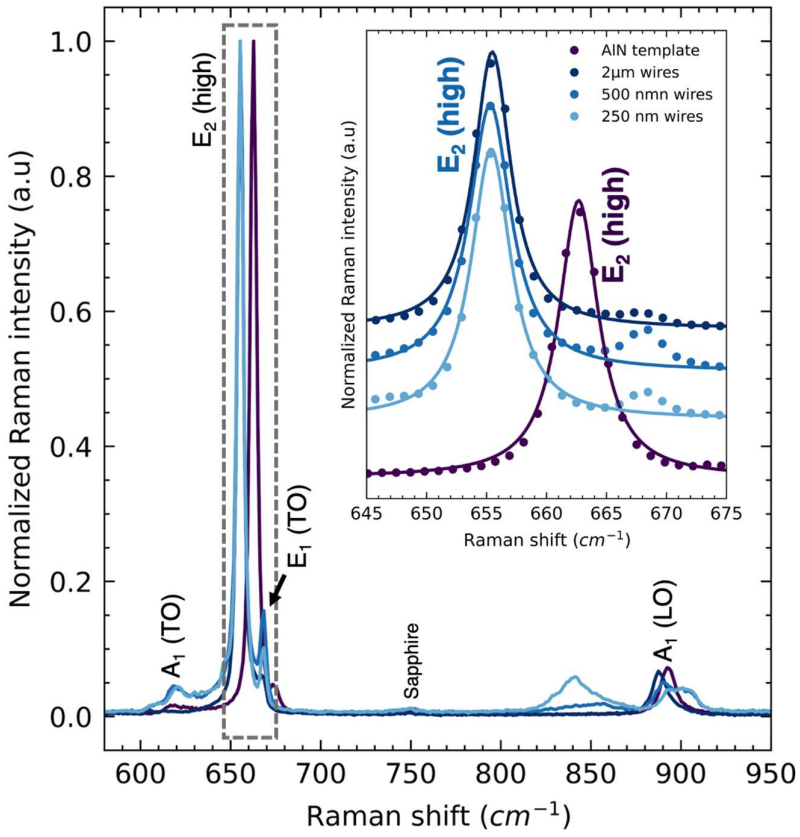

<u>Figure 2:</u> Micro-Raman spectra acquired on the AlN template as well as 2 µm, 500 nm and 250 nm wire arrays. The insert shows a zoom near the E_2(high) frequency. The experimental data (dots) are fitted on a lorentzian evolution (full line).

2. Optical properties of the pillars after the 1st step (top-down etching process)

Low temperature (5K) CL measurements are performed to investigate the effect of the top-down process on the AlN optical properties. The measurements are accomplished thanks to a field emission gun (FEG)-SEM with an embedded helium cryostat. The CL signal is collected by a parabolic mirror and is then analyzed by a charged-coupled device (CCD) with monochromator leading to a spectral resolution better than 1 meV. The CL spectra are measured under 3 kV acceleration voltage first on the AlN template before any process and second on a single AlN pillar (coming from the array : D = 500 nm, S = 5 µm) after the top-down process, as depicted in **Fig. 3(a)**. Also, the insert in **Fig. 3(a)** shows the full spectrum of the AlN template and the AlN pillar. Two contributions are visible for both spectra: one centered at 6.01 eV attributed to near band edge (NBE) emission of AlN and the other one, called the near UV band (NUVB), which is a defect band centered around 3.5 eV attributed to oxygen incorporation.[37] The intensity of the NUVB is lower for the AlN pillars compared to the AlN template. The AlN pillar-based sample being processed most recently, this characteristic can be attributed to the ageing of the sample, as AlN is known to oxidize over time.[38,39] A zoom close to the AlN near band edge (NBE) zone (5.7-6.2 eV) allows us to distinguish multiple contributions from both spectra. Temperature dependent CL study of the AlN NBE for the AlN template (see **Fig. S2** in Supplementary Materials) have led to the identification of the free exciton band at 6.090 eV. The other contributions are identified after referring the value of $\Delta E\ (\Gamma_5^{n=1})$ to the literature and are listed in **Tab. 1**.

Transition	E (eV)		FWHM (meV)		$\Delta E\ (\Gamma_5^{n=1})$ (meV)		$\Delta E_{lit}\ (\Gamma_5^{n=1})$ (meV)
	AlN pillar	AlN template	AlN pillar	AlN template	AlN pillar	AlN template	
$\Gamma_5^{n=1} - 2LO$	5.796		5.7		-241		-223[40], -231[41]
$\Gamma_5^{n=2} - 2LO$	5.834		8.7		-203		-189[40], -196[41]
$\Gamma_5^{n=1} - LO$	5.913		7.2		-124		-112[40], -119[41]
$\Gamma_5^{n=2} - LO$	5.953		11.1		-84		-73[40], -80[41]
D^0X_α	5.998	6.053	4.5	6.6	-39	-37	-37[40]
D^0X_1	6.007	6.058	1.7	2.6	-30	-32	-28[40], -28.5[42], -30[41],

							-28.7[43]05/06/2024 10:25:00
D^0X_β	6.016	6.066	2.7	2.3	-21	-24	-19[42], -23[41], -22[44], -22.4[43]
D^0X_2	6.023	6.075	1.5	2.9	-14	-15	-13[45], -13.3[42] , -14[41], -15[44], -13.4[43]
D^0X_γ	6.027	-	3.3		-10		-9.8[42]
$\Gamma_5^{n=1}$	6.037	6.090	3.0	2.8			
$\Gamma_5^{n=2}$	6.075	6.130	8.5	4.1	38	40	41[40], 39.4[42], 38.5[41], 39.3[43]

Table 1: identification of contributions measured in the CL spectra of the AlN template and the AlN pillar.

From LO phonon replica, we estimate the LO phonon energy to be around 120 meV. The energy splitting between the 1S and 2S excitonic states indicates an estimated binding energy of the exciton of 52 ± 2 meV, based on the Wannier-Mott exciton model. Such a value is consistent with the one found in the literature.[43,46] This high value of the exciton binding energy suggests that carrier recombination preserves an excitonic character up to room temperature. These microwires could therefore be used in the future as a platform for studying polaritons at room temperature.

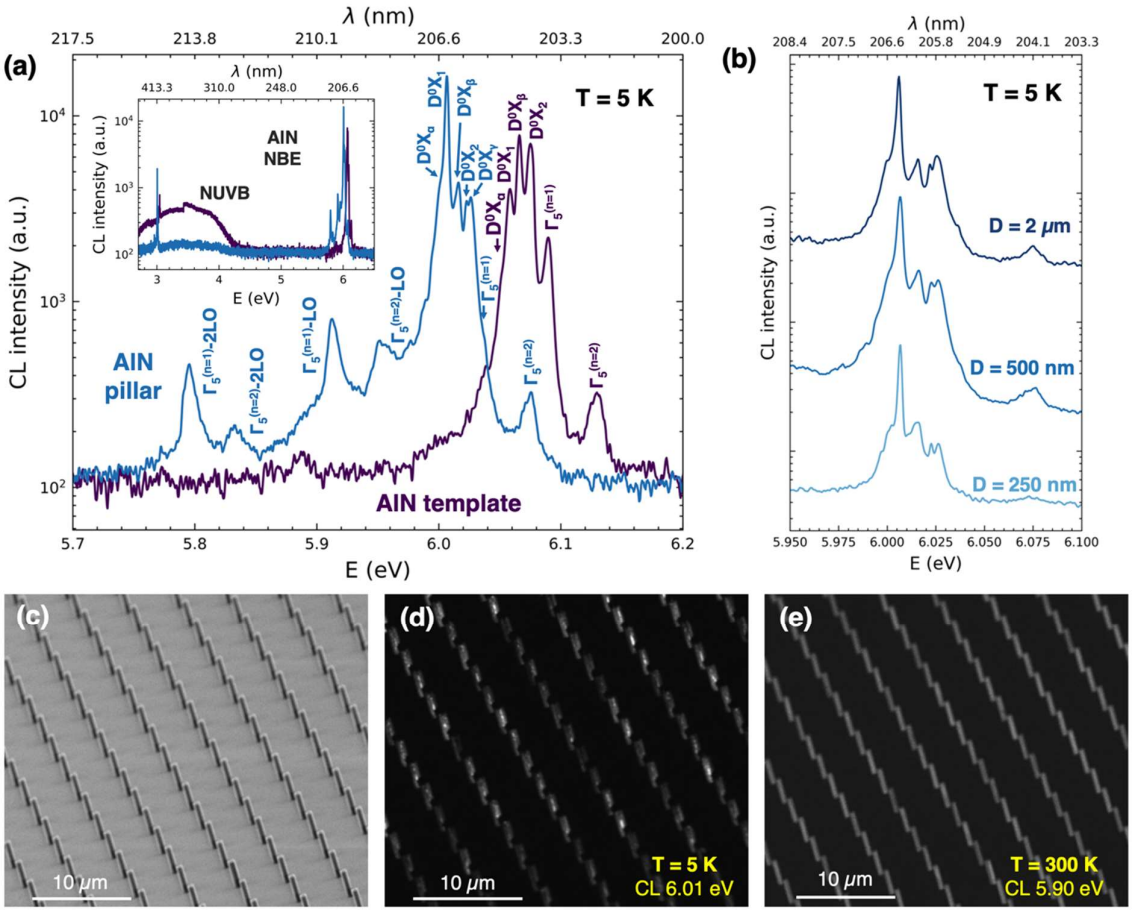

Figure 3: Optical study of AlN wires after the top-down process. (a) CL spectra near the NBE region acquired at 5 K for the AlN template and a single AlN wire (D = 500 nm; S = 5 µm). Their full spectrum are plotted in the insert. (b) CL spectra at 5K of single AlN wire measured on three different diameters : 2 µm, 500 nm and 250 nm. (c) Tilted SEM image of the array (D = 500 nm; S = 5 µm) and the corresponding PMT mappings (d) at 5 K centered around 6.01 eV and (e) at 300 K centered around 5.90 eV.

The NBE contributions of AlN pillar are redshifted by about ≈ 51 meV compared to those of the AlN template, which can be interpreted as the consequence of released strain. Moreover, this redshift is homogeneous along the sidewalls of a single AlN pillar (see **Fig. S3** in

Supplementary Materials) indicating a homogeneous strain relaxation. From literature, this shift corresponds approximately to a 0.19 % strain relaxation assuming biaxial strain.[47] This low value is consistent with the 0.38 %, previously found thanks to the micro-Raman analysis, indicating once again that the AlN template is already almost relaxed before the etching process.

Fig. 3(b) depicts three CL spectra measured at 5K for single pillars with 5 µm spacing and diameter of 2 µm, 500 nm and 250 nm, respectively. The same contributions are visible at the same emission energy for the three diameters considered. This feature is consistent with a small strain release after the top-down process that is independent of the diameter (this observation is in line with the position of the E_2 (high) mode in the Raman measurements, which was also independent of diameter).

Fig. 3(c) shows a SEM observation of a AlN pillar array (D = 500 nm and S = 5 µm) and the corresponding CL photo multiplicator tube (PMT) mapping at 5 K centered around 6.01 eV is shown in **Fig. 3(d)**. Even if all pillars exhibit AlN NBE emission, the intensity significantly fluctuates from wires to wires. As noticed in Fig. 3(a), D^0X_1 is the dominant contribution at low temperature, indicating that the donor incorporation at the origin of the D^0X_1 is inhomogeneous from wires to wires. In the literature, this donor has been identified to be either Si[48] or O[43] atoms. We assume that this contribution is less intense in AlN template because the etching process isolates a finite number of donor atoms (coming from the original AlN template) in a single AlN pillar, which leads to intensity differences and enhancement of the D^0X_1 contribution.

Fig. 3(e) shows the CL PMT mapping at 300 K of the AlN NBE centered around at 5.9 eV (see the full temperature study in **Fig. S4** in Supplementary Materials). In this case, the dominant contributions at room temperature are attributed to free carrier recombination and

D^0X_2 , asigned to exciton bound to native shallow donor in the literature[43]. Here, the emission is homogeneous along the pillars.

3. Focus on the 2nd process step: MOVPE AlN overgrowth

The MOVPE AlN overgrowth is handled in a closed coupled showerhead (3x2'') reactor. A 10 min annealing at 1200°C under H_2 atmosphere at 100 mbar prior to the growth is performed to remove contaminants due to air exposure. Here, two types of MOVPE growth conditions are investigated for the AlN overgrowth. First one is chosen to be similar to the usual growth conditions of planar *c*-oriented AlN[49,50]: growth under H_2 atmosphere at 1200 °C and 100 mbar using TMAl and NH_3 precursors with respective fluxes of 7.36 and 2 230 µmol.min^{-1} corresponding to a low V/III ratio equal to 300 (sample called "Low V/III"). Second one is the same except for the NH_3 flux, which is now 201 000 µmol.min^{-1} leading to a significant V/III ratio equal to 27 000 (sample called "High V/III"), in accordance with the already reported AlN overgrowth on wire geometry.[23,51] The growth time is 1 hour and 30 minutes for both samples, corresponding to the deposition of approximately 225 nm AlN for the "High V/III" recipe and 190 nm AlN for the "Low V/III" one (for the S =5 µm and $D_{initial}$ = 500 nm pillars). SEM observations of the samples after the MOVPE regrowth for both recipes and for three diameters (S = 5 µm ; $D_{initial}$ = 2 µm, 500 nm and 250 nm) are shown in **Fig. 4(a-f)**. The wires surfaces under low V/III (**Fig. 4(a-c)**) exhibit increased roughness for all diameter compared to the high V/III recipe (**Fig. 4(d-f)**). Anisotropic growth features, with elongated stripes along the *a*-axis, are clearly distinguishable on the *m*-surface sidewalls of AlN wires using the low V/III recipe. These features can be interpreted as a sign of poor Al adatom diffusion on the *m*-surface.[52] Indeed, in the case of the *m*-surfaces, a diffusion barrier along the *c*-axis exists for the Al adatom that enhances the diffusion along the *a*-axis.[53] On the contrary, such features are not visible on the *m*-surfaces of the AlN wires applying the high V/III recipe, indicating an

enhanced Al diffusion for these growth conditions. Nevertheless, edge recovery is not completed for all the wires with 2 µm initial diameter after the growth (See **Fig. S5** in Supplementary Materials). This characteristic, only visible for the largest diameter, can be interpreted as a consequence of a limited adatom diffusion, even along the *a*-axis. SEM observations with lower magnification of two arrays after the MOVPE growth ($D_{initial}$ = 500 nm and S = 2 and 5 µm) shown in **Fig. 4(g-h)** emphasizes the good homogeneity from wires to wires.

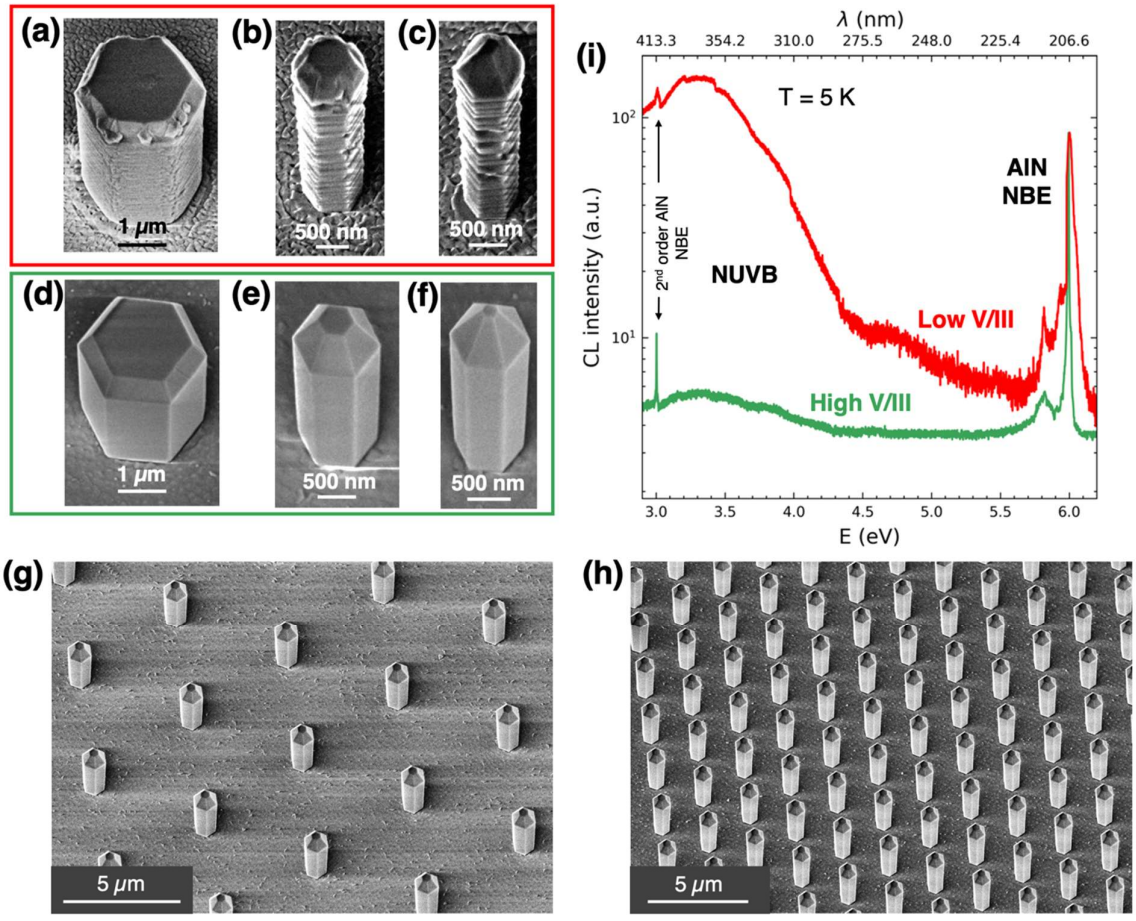

Figure 4: Optimization of MOVPE AlN regrowth conditions. SEM images of the AlN wires (with $D_{initial}$ = 2 µm, 500 nm and 250 nm) after the MOVPE regrowth using (a-c) low V/III ratio recipe and (d-f) high V/III ratio recipe. SEM images with lower magnification of two different

arrays after the high V/III ratio MOVPE regrowth: (g) $D_{initial}$ = 500 nm, S = 5 µm and (h) $D_{initial}$ = 500 nm, S = 2 µm. (i) CL spectra measured at 5K on a single AlN wire ($D_{initial}$ = 500 nm; S = 5 µm) after the MOVPE regrowth using low and high V/III recipes. Both spectra are normalized compared to the intensity of the AlN NBE.

After the MOVPE overgrowth, CL measurements at 5K on both samples are performed on an single AlN wire ($D_{initial}$ = 500 nm and S = 5 µm). Spectra, represented in **Fig. 4(i)**, are measured with 3kV acceleration voltage to ensure to only probe the MOVPE regrown AlN (an estimated 90 nm CL probing depth is computed using the software CASINO).[54] Both spectra exhibit again two contributions: the AlN NBE emission centered around 6 eV and the NUVB centered around 3.5 eV (the intensities are normalized on the AlN NBE intensity for both spectra). NUVB intensity is significantly higher for the low V/III recipe (the NBE/NUVB intensity ratio equal to 0.55 and 15 for low V/III and high V/III samples). The improved optical properties are therefore consistent with the better morphology of the AlN wires grown with the high V/III recipe.

4. Growth mechanism of organized wires

Fig. 5 shows top-view SEM pictures of AlN wires before (**Fig. 5 (a-c)**) and after (**Fig. 5 (d-f)**) the MOVPE growth for three initial diameters equal respectively to 2 µm, 500 and 250 nm (S = 5 µm). The hexagonal facets are completely recovered exhibiting *m*-plane facets for all the diameters. Comparing final and initial diameters of AlN wires after MOVPE overgrowth, the lateral growth rate is estimated on *m*-facets, as a function of diameter (2 and 1 µm, 500, 350 and 250 nm) and spacing (15, 5 and 2 µm) and these data are plotted in **Fig. 5(g)**. We note that the growth rate of *m*-plane facets follows a non-linear evolution for both pitch and diameter.

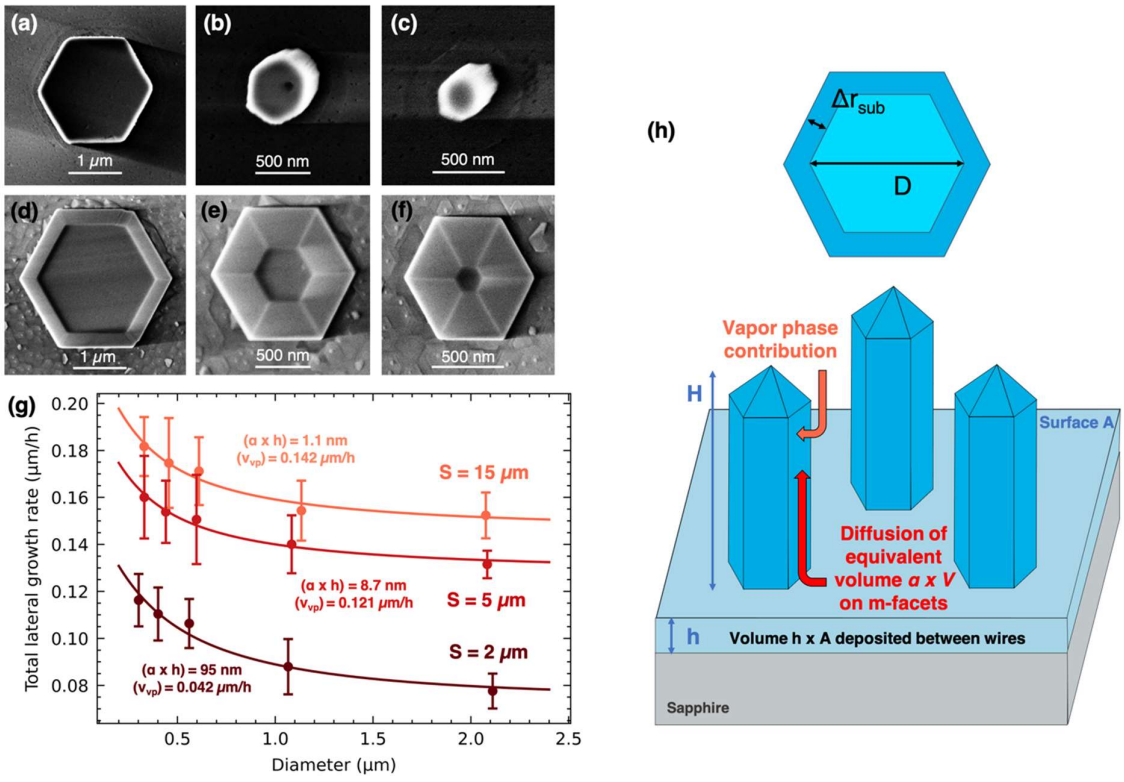

Figure 5: Top-view SEM images of single AlN wire with three diameters (D = 2 µm, 500 nm and 250 nm) (a-c) before and (d-f) after the MOVPE re-growth. (g) Evolution of the speed

growth as a function of initial diameter for three spacings : 2, 5 and 15 µm. Experimental data represented by dots are fitted by full lines based on the developed growth model. (h) Schematic of the growth mechanism in place during the MOVPE regrowth with explicit parameters used in the growth model.

To explain this behavior, a growth model is established hereafter. To model the evolution of the lateral growth rate of AlN wires, we consider that the total lateral growth rate v_{total} results from two distinguished contributions:

$$v_{total}(D,S) = v_{vp}(S) + v_{sub}(D,S) \quad (1)$$

v_{vp} is the growth rate from species coming from the vapor phase and v_{sub} is the growth rate from adatoms coming from the substrate by surface diffusion.

V_{vp} is considered to be dependent of the spacing S of the considered array. Indeed, in those growth conditions, the surface reactions occurring on the *m*-facets of a single wire to grow AlN are assumed to be limited by the low flux of TMAl in consideration of the massive flux of NH_3. Thus, the low amount of TMAl available in the vapor phase is shared between all the wires. Therefore, the contribution v_{vp} is expected to vary as a function of the wire density and so, as a function of the spacing S.

V_{sub} is considered to be dependent of spacing and diameter. V_{sub} is simply defined as follow:

$$v_{sub} = \frac{\Delta r_{sub}}{\Delta t} \quad (2)$$

where Δr_{sub} is the increase of the AlN wire radius corresponding to the substrate contribution and Δt the growth duration. The value of Δr_{sub} is assumed to be directly linked to the amount of Al adatoms deposited between wires. Actually, only a fraction of the adatoms deposited between wires diffuses towards the m-facets of the wires and contributes to the lateral growth, as depicted in the schematic **Fig. 5(h)**.

This assumption is expressed in the form of the following equation:

$$\alpha \times V = N \times V_{AlN}^{Diff} \quad (3)$$

where α is the fraction of the equivalent volume V deposited between wires that will diffuse on the *m*-facets, N is the number of AlN wires, and V_{AlN}^{Diff} corresponds to the difference of expended volume for one AlN wire considering only the substrate diffusion. The equation (3) can be written as follow considering a hexagonal shape for AlN wires:

$$\alpha \times V = N \times H \times \frac{\sqrt{3}}{2}[(D + 2 \times \Delta r_{sub})^2 - D^2] \quad (4)$$

where H is the height of the AlN wires and D the diameter. The number of wires N in a considered surface A is expressed as:

$$N = \frac{A}{(D+S)^2} \quad (5)$$

where *S* is the spacing of the considered array. Volume between wires V for the same surface A is written as:

$$V = h \times A - N \times h \times \frac{\sqrt{3}}{2} D^2 \quad (6)$$

where h is the thickness of the AlN deposition between wires.

From equation (4), using the expression (5) and (6), Δr_{sub} is expressed as a function of D and S:

$$\Delta r_{sub}(D,S) = \frac{1}{2}\sqrt{\frac{2\sqrt{3}}{3}\frac{\alpha \times h}{H}(D+S)^2 + (1 - \frac{\alpha \times h}{H})D^2} - \frac{D}{2}$$

Using the equation (2), the growth rate from substrate diffusion is equal to:

$$v_{sub}(D,S) = \frac{1}{\Delta t}\left[\frac{1}{2}\sqrt{\frac{2\sqrt{3}}{3}\frac{\alpha \times h}{H}(D+S)^2 + (1-\frac{\alpha \times h}{H})D^2} - \frac{D}{2}\right]$$

Finally, we can express the equation of total lateral growth rate:

$$v_{total}(D,S) = v_{vp}(S) + \frac{1}{\Delta t}\left[\frac{1}{2}\sqrt{\frac{2\sqrt{3}}{3}\frac{\alpha \times h}{H}(D+S)^2 + (1-\frac{\alpha \times h}{H})D^2} - \frac{D}{2}\right]$$

The growth rates determined experimentally for each pitch are fitted using this model. Here, Δt is equal to 1h 30 min and H to 3 µm. The free parameters of the model "α x h" and v_{vp} obtained after fitting the data, as well as the percentage of each contribution (v_{vp} and v_{sub}) compared to v_{total}, are given in **Tab. 2** for each spacing value.

Spacing value (µm)	"α x h" (nm)	v_{vp} (µm.h^{-1})	v_{vp}/v_{total} (%)	v_{sub}/v_{total} (%)
2	95	0.042	32-52 %	48-68 %
5	8.7	0.121	69-90 %	10-31 %
15	1.1	0.142	71-95 %	5-39 %

Table 2: Parameters "α x h" and v_{vp} obtained after fitting the data to the growth model for the three spacings (S = 2, 5 and 15 µm) and percentage of the v_p and v_{sub} contributions compared to v_{total}.

It is worth noticing that by using those growth conditions (high V/III ratio), the substrate contribution is far from being negligeable. This phenomenon is also enhanced for the smallest diameter, the substrate contribution being the main one for the wires with $D_{initial}$ = 250 nm and S = 2 µm (68% compared to v_{total}).

The fitted value of v_{vp}, as well as its percentage compared to v_{total}, decreases as the spacing decreases, which is coherent with the earlier assumption that the vapor phase is shared between wires. The fitted value of "α x h", as well as the v_{sub} percentage compared to v_{total}, increases as the spacing decreases. This indicates than a higher fraction of the adatoms deposited between the wires diffuses to the *m*-plane facets and contributes to the growth in the case of a denser array. This feature is attributed to the relatively short diffusion length usually observed for Al adatoms, limiting the amount of Al adatoms coming from the Al diffusion on the substrate in the case of large spacing.[55,56]

5. Optical properties of wires after the 2nd step (AlN overgrowth)

The optical properties of the AlN wires after the MOVPE growth are investigated using CL at 5K. The spectral analysis of a typical single AlN wire (with $D_{initial}$ = 500 nm and S = 5 µm) before and after the MOVPE growth are depicted in **Fig. 6(a)**. The intensity spectra have been normalized on the AlN NBE intensity for clearer visualization.

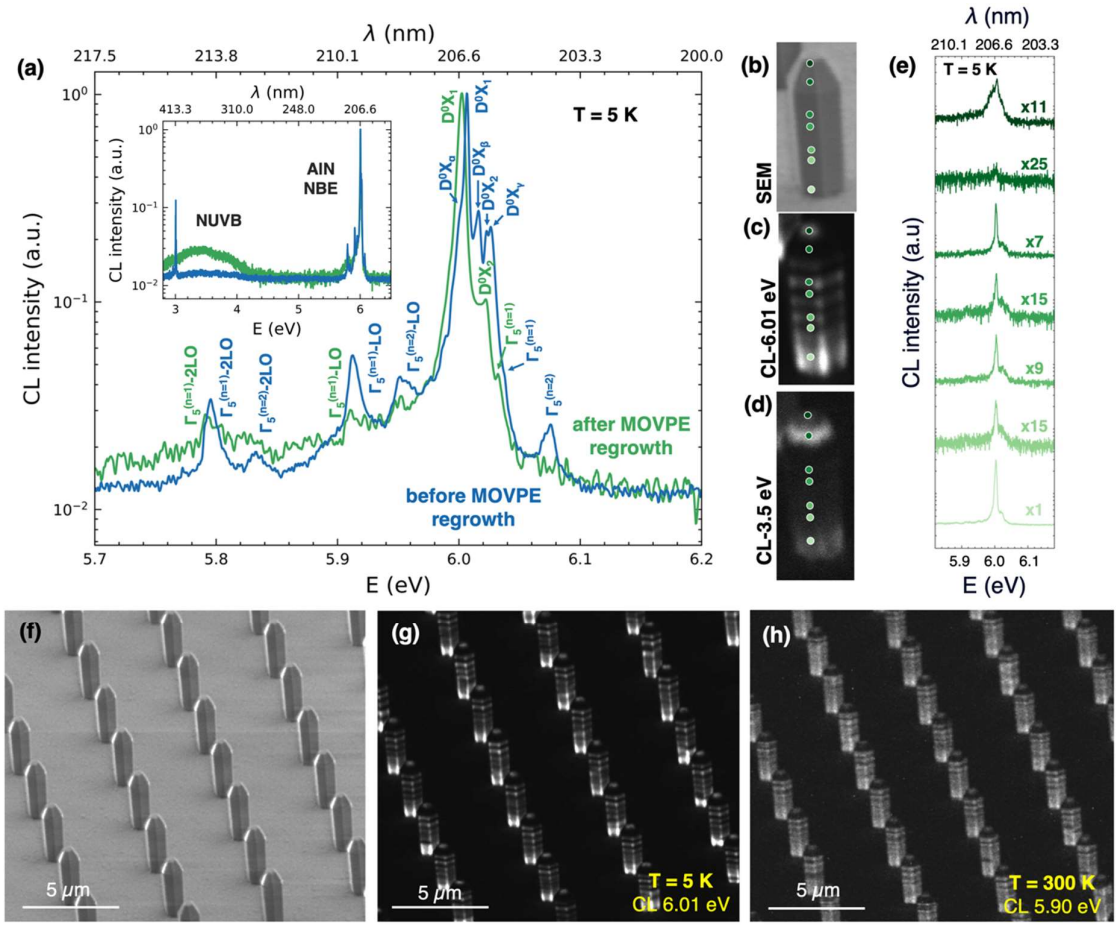

<u>Figure 6:</u> Optical study of AlN wires after the AlN regrowth process. (a) CL spectra near the NBE region acquired at 5 K for a single wire (D = 500 nm; S = 5 µm) before and after the MOVPE regrowth. Their full spectrum is plotted in the insert. (b) SEM image of a single AlN wire after the MOVPE regrowth ($D_{initial}$ = 500 nm and S = 5 µm) and corresponding PMT mapping acquired at 5K centered around (c) 6.01 eV and (d) 3.5 eV. (e) CL spectrum acquired

in spot mode along the wire sidewall. Fit between SEM image, PMT mappings and CL spectrum are highlighted by green dots, which have the same green nuance that the corresponding CL spot spectra. (f) Tilted SEM image of one array (D = 500 nm; S = 5 µm) and the corresponding PMT mapping (g) at 5 K centered around 6.01 eV and (h) at 300 K centered around 5.90 eV.

The insert of **Fig. 6(a)** shows the full spectra for both samples. The NUVB contribution is enhanced after the MOVPE growth (the ratio NBE/NUVB changes from 65 to 32 before and after the growth). The NUVB being attributed to oxygen, this enhancement could be explained by the incorporation of residual O inside the MOVPE reactor during the growth. The **Fig. 6(a)** shows the CL spectra of the AlN at the NBE region, allowing to distinguish multiple contributions. The contributions are identified, as before, by comparing the energy position of the contribution to the energy of free excitons in the sample. The results are summarized in **Tab. 3**.

Transition	E (eV)		FWHM (meV)		ΔE ($\Gamma_5^{n=1}$) (meV)		ΔE_{lit} ($\Gamma_5^{n=1}$) (meV)
	AlN wires before MOVPE growth	AlN wires after MOVPE growth	AlN wires before MOVPE growth	AlN wires after MOVPE growth	AlN wires before MOVPE growth	AlN wires after MOVPE growth	
$\Gamma_5^{n=1} - 2LO$	5.796	5.795	5.7	5.8	-241	-238	-223[40], -231[41]
$\Gamma_5^{n=2} - 2LO$	5.834		8.7		-203		-189[40], -196[41]
$\Gamma_5^{n=1} - LO$	5.913	5.914	7.2	6.0	-124	-119	-112[40], -119[41]
$\Gamma_5^{n=2} - LO$	5.953		11.1		-84		-73[40], -80[41]
D^0X_α	5.998		4.5		-39		-37[40]
D^0X_1	6.007	6.002	1.7	3.2	-30	-31	-28[40], -28.5[42], -30[41], -28.7[43]05/06/2024 10:25:00
D^0X_β	6.016		2.7		-21		-19[42], -23[41], -22[44], -22.4[43]
D^0X_2	6.023		1.5		-14		-13[40], -13.3[42] , -14[41], -15[44], -13.4[43]
D^0X_γ	6.027	6.022	3.3	3.8	-10	-11	-9.8[42]
$\Gamma_5^{n=1}$	6.037	6.033	3.0	3.0			
$\Gamma_5^{n=2}$	6.075		8.5		38		41[40], 39.4[42], 38.5[41], 39.3[43]

Table 3: Identification of contributions observed in the CL spectra from single AlN wire after MOVPE overgrowth.

A small shift (4 meV) of the free exciton contribution is measured between the samples before and after the MOVPE growth. This shift is found to be equal for the different diameters but inhomogeneous along the wire sidewalls (See **Fig. S6** and **S7** in Supplementary materials). **Fig. 6(b)** shows the SEM picture of a AlN wire ($D_{initial}$ = 500 nm and S = 5 µm). A very slight broadening of the peaks can be observed after growth, indicating that the crystalline quality of the material undergoes very little alteration during the MOVPE regrowth. The associated PMT mappings centered around 6.01 eV and 3.5 eV are respectively displayed in **Fig. 6(c)** and **Fig. 6(d)**. The intensity of AlN NBE emission is inhomogeneous along the m-planes of the wire. First, "ring-like" emission with brighter or darker AlN NBE emission intensity are distinguishable around the AlN wire. Second, the AlN NBE intensity is enhanced near the edges and at the bottom part of the wire. The PMT mapping associated to NUVB represented **Fig. 6(d)** reveals that this contribution is also inhomogeneous along the AlN wire. The intensity is brighter at the bottom part of the AlN wire and on semi-polar facets. This feature could be interpreted as an enhanced O incorporation on semi-polar facets, similar to GaN, where this phenomenon has previously been observed.[57] Spectrum acquired in spot mode along different location on the wire sidewall are represented in **Fig. 6(e)**. The fit between the SEM picture and the two PMT mappings are highlighted on **Fig. 6(b-d)** by green dots, which are the same nuance of their corresponding spot spectra in **Fig. 6(e)**. Thus, AlN NBE emission is measured on the full *m*-plane surface (even on "dark ring" zones) except on the semi-polar facets, where the NBE is almost undistinguishable. This feature is certainly explained by a reduced-quality AlN epitaxy on semi-polar facets, which is consistent with the enhanced intensity of the NUVB contribution on those facets. The reduction of the crystal quality epitaxy

on *c*-plane can also be deduced by the enlargement of the AlN NBE emission in this region. It confirms that the growth conditions chosen for the MOVPE overgrowth are optimized for *m*-plane growth.

In addition, CL are performed on a large zone of the organized AlN wire arrays. **Fig. 6(g)** represents the PMT mapping at 5 K centered around the AlN NBE (6.01 eV) of one AlN array ($D_{initial}$ = 500 nm and S = 5 µm) and its corresponding SEM image in **Fig. 6(f)**. The "ring-like" feature described above is present for all the wires included in the PMT mapping, without noticeable variation of intensity from wire-to-wire. Also, the corresponding PMT mapping at room temperature (around 5.9 eV) is plotted in **Fig. 6(h)**, still revealing "ring-like" features on all the wires (see the full temperature study acquired on a single wire in **Fig. S8** in Supplementary Materials). These "intensity rings" present on the wires after the MOVPE overgrowth can be interpreted as the result of poor Al adatom diffusion along the *a*-axis. Indeed, even if the rough morphology observed in **Fig. 4(a-c)** has been smoothen out after the growth conditions optimization, the preferential growth along the *a*-axis may still occurs.

Conclusion

In conclusion, AlN microwire arrays are successfully fabricated combining top-down etching (using both plasma and KOH etching) and AlN overgrowth by MOVPE. MOVPE AlN regrowth conditions are optimized and a high V/III ratio (27 000) is found mandatory to achieve AlN wires with smooth m-facet sidewalls. The lateral growth rate of AlN depends on the wire spacing and diameter, which is modelled considering both the direct growth from vapor phase and the adatom diffusion from the substrate. Moreover, CL measurements highlight that the NBE emission of AlN is maintained up to room temperature through the entire process. The narrow width at half-height of the NBE peaks after MOVPE overgrowth demonstrates the high crystalline quality of the epitaxial AlN. This work paves the way for novel UV emitters design based on such AlN microwire arrays, taking advantages of the strain-free state of the AlN microwires and the identical optical and morphological properties regardless of diameter and spacing of the arrays.

Supporting Information

Additionnal SEM observations of the AlN microwire arrays before and after the MOVPE overgrowth, CL measurements as a function of the position on the AlN wire sidewalls, temperature dependant CL studies on the AlN microwires emission (PDF).

Acknowledgement

This research was funded by the French National Research Agency in the framework of the program ANR-22-CE51-0032-01 and the French National Research Agency in the framework of the "Investissements d’avenir” program (ANR-15-IDEX-02). It was also supported by the French RENATECH network.

References

[1] H.L. Bank, J. John, M.K. Schmehl, and R.J. Dratch, "Bactericidal effectiveness of modulated UV light," Appl. Environ. Microbiol. **56**(12), 3888–3889 (1990).
[2] N. Vermeulen, W.J. Keeler, K. Nandakumar, and K.T. Leung, "The bactericidal effect of ultraviolet and visible light onEscherichia coli," Biotechnol. Bioeng. **99**(3), 550–556 (2008).
[3] S. Vilhunen, H. Särkkä, and M. Sillanpää, "Ultraviolet light-emitting diodes in water disinfection," Environ. Sci. Pollut. Res. **16**(4), 439–442 (2009).
[4] M.A. Würtele, T. Kolbe, M. Lipsz, A. Külberg, M. Weyers, M. Kneissl, and M. Jekel, "Application of GaN-based ultraviolet-C light emitting diodes – UV LEDs – for water disinfection," Water Res. **45**(3), 1481–1489 (2011).
[5] H. Amano, R. Collazo, C.D. Santi, S. Einfeldt, M. Funato, J. Glaab, S. Hagedorn, A. Hirano, H. Hirayama, R. Ishii, Y. Kashima, Y. Kawakami, R. Kirste, M. Kneissl, R. Martin, F. Mehnke, M. Meneghini, A. Ougazzaden, P.J. Parbrook, S. Rajan, P. Reddy, F. Römer, J. Ruschel, B. Sarkar, F. Scholz, L.J. Schowalter, P. Shields, Z. Sitar, L. Sulmoni, T. Wang, T. Wernicke, M. Weyers, B. Witzigmann, Y.-R. Wu, T. Wunderer, and Y. Zhang, "The 2020 UV emitter roadmap," J. Phys. Appl. Phys. **53**(50), 503001 (2020).
[6] P. Pampili, and P.J. Parbrook, "Doping of III-nitride materials," Mater. Sci. Semicond. Process. **62**, 180–191 (2017).
[7] K.B. Nam, M.L. Nakarmi, J. Li, J.Y. Lin, and H.X. Jiang, "Mg acceptor level in AlN probed by deep ultraviolet photoluminescence," Appl. Phys. Lett. **83**(5), 878–880 (2003).
[8] M.L. Nakarmi, K.H. Kim, K. Zhu, J.Y. Lin, and H.X. Jiang, "Transport properties of highly conductive n-type Al-rich AlxGa1−xN(x⩾0.7)," Appl. Phys. Lett. **85**(17), 3769–3771 (2004).
[9] T.A. Henry, A. Armstrong, A.A. Allerman, and M.H. Crawford, "The influence of Al composition on point defect incorporation in AlGaN," Appl. Phys. Lett. **100**(4), 043509 (2012).
[10] H.-Y. Ryu, I.-G. Choi, H.-S. Choi, and J.-I. Shim, "Investigation of Light Extraction Efficiency in AlGaN Deep-Ultraviolet Light-Emitting Diodes," Appl. Phys. Express **6**(6), 062101 (2013).
[11] J. Bai, T. Wang, P.J. Parbrook, K.B. Lee, and A.G. Cullis, "A study of dislocations in AlN and GaN films grown on sapphire substrates," J. Cryst. Growth **282**(3–4), 290–296 (2005).
[12] S.D. Hersee, A.K. Rishinaramangalam, M.N. Fairchild, L. Zhang, and P. Varangis, "Threading defect elimination in GaN nanowires," J. Mater. Res. **26**(17), 2293–2298 (2011).
[13] P.M. Coulon, M. Mexis, M. Teisseire, M. Jublot, P. Vennéguès, M. Leroux, and J. Zuniga-Perez, "Dual-polarity GaN micropillars grown by metalorganic vapour phase epitaxy: Cross-correlation between structural and optical properties," J. Appl. Phys. **115**(15), 153504 (2014).
[14] V. Grenier, S. Finot, G. Jacopin, C. Bougerol, E. Robin, N. Mollard, B. Gayral, E. Monroy, J. Eymery, and C. Durand, "UV Emission from GaN Wires with *m* -Plane Core–Shell GaN/AlGaN Multiple Quantum Wells," ACS Appl. Mater. Interfaces **12**(39), 44007–44016 (2020).
[15] M. Djavid, and Z. Mi, "Enhancing the light extraction efficiency of AlGaN deep ultraviolet light emitting diodes by using nanowire structures," Appl. Phys. Lett. **108**(5), 051102 (2016).
[16] D. Lee, J.W. Lee, J. Jang, I.-S. Shin, L. Jin, J.H. Park, J. Kim, J. Lee, H.-S. Noh, Y.-I. Kim, Y. Park, G.-D. Lee, Y. Park, J.K. Kim, and E. Yoon, "Improved performance of AlGaN-based deep ultraviolet light-emitting diodes with nano-patterned AlN/sapphire substrates," Appl. Phys. Lett. **110**(19), 191103 (2017).
[17] J. Rass, H.K. Cho, M. Guttmann, D. Prasai, J. Ruschel, T. Kolbe, and S. Einfeldt, "Enhanced light extraction efficiency of far-ultraviolet-C LEDs by micro-LED array design," Appl. Phys. Lett. **122**(26), 263508 (2023).

[18] H. Spende, C. Margenfeld, and A. Waag, "AlGaN Microfins as Nonpolar UV Emitters Probed by Time-Resolved Cathodoluminescence," ACS Photonics **9**(5), 1594–1604 (2022).
[19] V. Grenier, S. Finot, L. Valera, J. Eymery, G. Jacopin, and C. Durand, "UV-A to UV-B electroluminescence of core-shell GaN/AlGaN wire heterostructures," Appl. Phys. Lett. **121**(13), 131102 (2022).
[20] L. Valera, V. Grenier, S. Finot, C. Bougerol, J. Eymery, G. Jacopin, and C. Durand, "*M* -plane AlGaN digital alloy for microwire UV-B LEDs," Appl. Phys. Lett. **122**(14), 141101 (2023).
[21] Y. Ra, S. Kang, and C. Lee, "Ultraviolet Light-Emitting Diode Using Nonpolar AlGaN Core–Shell Nanowire Heterostructures," Adv. Opt. Mater. **6**(14), 1701391 (2018).
[22] V. Grenier, S. Finot, B. Gayral, C. Bougerol, G. Jacopin, J. Eymery, and C. Durand, "Toward Crack-Free Core–Shell GaN/AlGaN Quantum Wells," Cryst. Growth Des. **21**(11), 6504–6511 (2021).
[23] P.-M. Coulon, G. Kusch, P. Fletcher, P. Chausse, R. Martin, and P. Shields, "Hybrid Top-Down/Bottom-Up Fabrication of a Highly Uniform and Organized Faceted AlN Nanorod Scaffold," Materials **11**(7), 1140 (2018).
[24] L. Jaloustre, V. Ackermann, S. Sales De Mello, S. Labau, C. Petit-Etienne, and E. Pargon, "Preferential crystal orientation etching of GaN nanopillars in Cl2 plasma," Mater. Sci. Semicond. Process. **165**, 107654 (2023).
[25] L. Jaloustre, S. Sales De Mello, S. Labau, C. Petit-Etienne, and E. Pargon, "Faceting mechanisms of GaN nanopillar under KOH wet etching," Mater. Sci. Semicond. Process. **173**, 108095 (2024).
[26] J. Gleize, M.A. Renucci, J. Frandon, E. Bellet-Amalric, and B. Daudin, "Phonon deformation potentials of wurtzite AlN," J. Appl. Phys. **93**(4), 2065–2068 (2003).
[27] T. Prokofyeva, M. Seon, J. Vanbuskirk, M. Holtz, S.A. Nikishin, N.N. Faleev, H. Temkin, and S. Zollner, "Vibrational properties of AlN grown on (111)-oriented silicon," Phys. Rev. B **63**(12), 125313 (2001).
[28] U. Haboeck, H. Siegle, A. Hoffmann, and C. Thomsen, "Lattice dynamics in GaN and AlN probed with first- and second-order Raman spectroscopy," Phys. Status Solidi C (6), 1710–1731 (2003).
[29] M. Kadleíková, J. Breza, and M. Veselý, "Raman spectra of synthetic sapphire," Microelectron. J. **32**(12), 955–958 (2001).
[30] A.R. Goñi, H. Siegle, K. Syassen, C. Thomsen, and J.-M. Wagner, "Effect of pressure on optical phonon modes and transverse effective charges in GaN and AlN," Phys. Rev. B **64**(3), 035205 (2001).
[31] H.J. Trodahl, F. Martin, P. Muralt, and N. Setter, "Raman spectroscopy of sputtered AlN films: E2(high) biaxial strain dependence," Appl. Phys. Lett. **89**(6), 061905 (2006).
[32] V. Lughi, and D.R. Clarke, "Defect and stress characterization of AlN films by Raman spectroscopy," Appl. Phys. Lett. **89**(24), 241911 (2006).
[33] X. Rong, X. Wang, G. Chen, J. Pan, P. Wang, H. Liu, F. Xu, P. Tan, and B. Shen, "Residual stress in AlN films grown on sapphire substrates by molecular beam epitaxy," Superlattices Microstruct. **93**, 27–31 (2016).
[34] C. Durand, C. Bougerol, J.-F. Carlin, G. Rossbach, F. Godel, J. Eymery, P.-H. Jouneau, A. Mukhtarova, R. Butté, and N. Grandjean, "*M* -Plane GaN/InAlN Multiple Quantum Wells in Core–Shell Wire Structure for UV Emission," ACS Photonics **1**(1), 38–46 (2014).
[35] A.V. Kuchuk, F.M. De Oliveira, P.K. Ghosh, Y.I. Mazur, H.V. Stanchu, M.D. Teodoro, M.E. Ware, and G.J. Salamo, "Coherent-interface-induced strain in large lattice-mismatched materials: A new approach for modeling Raman shift," Nano Res. **15**(3), 2405–2412 (2022).
[36] S. Yang, R. Miyagawa, H. Miyake, K. Hiramatsu, and H. Harima, "Raman Scattering Spectroscopy of Residual Stresses in Epitaxial AlN Films," Appl. Phys. Express **4**(3), 031001

(2011).
[37] I.A. Weinstein, A.S. Vokhmintsev, and D.M. Spiridonov, "Thermoluminescence kinetics of oxygen-related centers in AlN single crystals," Diam. Relat. Mater. **25**, 59–62 (2012).
[38] P. Bowen, J.G. Highfield, A. Mocellin, and T.A. Ring, "Degradation of Aluminum Nitride Powder in an Aqueous Environmet," J. Am. Ceram. Soc. **73**(3), 724–728 (1990).
[39] J. Li, M. Nakamura, T. Shirai, K. Matsumaru, C. Ishizaki, and K. Ishizaki, "Mechanism and Kinetics of Aluminum Nitride Powder Degradation in Moist Air," J. Am. Ceram. Soc. **89**(3), 937–943 (2006).
[40] L. van Deurzen, J. Singhal, J. Encomendero, N. Pieczulewski, C. Chang, Y. Cho, D.A. Muller, H.G. Xing, D. Jena, O. Brandt, and J. Lähnemann, "Excitonic and deep-level emission from N- and Al-polar homoepitaxial AlN grown by molecular beam epitaxy," (2023).
[41] T. Onuma, T. Shibata, K. Kosaka, K. Asai, S. Sumiya, M. Tanaka, T. Sota, A. Uedono, and S.F. Chichibu, "Free and bound exciton fine structures in AlN epilayers grown by low-pressure metalorganic vapor phase epitaxy," J. Appl. Phys. **105**(2), 023529 (2009).
[42] B. Neuschl, K. Thonke, M. Feneberg, S. Mita, J. Xie, R. Dalmau, R. Collazo, and Z. Sitar, "Optical identification of silicon as a shallow donor in MOVPE grown homoepitaxial AlN," Phys. Status Solidi B **249**(3), 511–515 (2012).
[43] M. Feneberg, B. Neuschl, K. Thonke, R. Collazo, A. Rice, Z. Sitar, R. Dalmau, J. Xie, S. Mita, and R. Goldhahn, "Sharp bound and free exciton lines from homoepitaxial AlN: Sharp bound excitons from AlN," Phys. Status Solidi A **208**(7), 1520–1522 (2011).
[44] E. Silveira, J.A. Freitas, M. Kneissl, D.W. Treat, N.M. Johnson, G.A. Slack, and L.J. Schowalter, "Near-bandedge cathodoluminescence of an AlN homoepitaxial film," Appl. Phys. Lett. **84**(18), 3501–3503 (2004).
[45] R. Ishii, T. Nagashima, R. Yamamoto, T. Hitomi, M. Funato, and Y. Kawakami, "Stimulated emission mechanism of aluminum nitride," Phys. Rev. B **105**(20), 205206 (2022).
[46] M. Feneberg, R.A.R. Leute, B. Neuschl, K. Thonke, and M. Bickermann, "High-excitation and high-resolution photoluminescence spectra of bulk AlN," Phys. Rev. B **82**(7), 075208 (2010).
[47] G. Rossbach, M. Feneberg, M. Röppischer, C. Werner, N. Esser, C. Cobet, T. Meisch, K. Thonke, A. Dadgar, J. Bläsing, A. Krost, and R. Goldhahn, "Influence of exciton-phonon coupling and strain on the anisotropic optical response of wurtzite AlN around the band edge," Phys. Rev. B **83**(19), 195202 (2011).
[48] H. Murotani, R. Tanabe, K. Hisanaga, A. Hamada, K. Beppu, N. Maeda, M.A. Khan, M. Jo, H. Hirayama, and Y. Yamada, "High internal quantum efficiency and optically pumped stimulated emission in AlGaN-based UV-C multiple quantum wells," Appl. Phys. Lett. **117**(16), 162106 (2020).
[49] V.Z. Zubialevich, P. Pampili, and P.J. Parbrook, "Fast Growth of Smooth AlN in a 3 × 2″ Showerhead-Type Vertical Flow MOVPE Reactor," Phys. Status Solidi B **255**(5), 1700472 (2018).
[50] Y. Ohba, and R. Sato, "Growth of AlN on sapphire substrates by using a thin AlN bu!er layer grown two-dimensionally at a very low V/III ratio," J. Cryst. Growth, (2000).
[51] R. Armstrong, P.-M. Coulon, P. Bozinakis, R.W. Martin, and P.A. Shields, "Creation of regular arrays of faceted AlN nanostructures via a combined top-down, bottom-up approach," J. Cryst. Growth **548**, 125824 (2020).
[52] S. Adhikari, F. Kremer, M. Lysevych, C. Jagadish, and H.H. Tan, "Core–shell GaN/AlGaN nanowires grown by selective area epitaxy," Nanoscale Horiz., 10.1039.D2NH00500J (2023).
[53] V. Jindal, and F. Shahedipour-Sandvik, "Density functional theoretical study of surface structure and adatom kinetics for wurtzite AlN," J. Appl. Phys. **105**(8), 084902 (2009).

[54] D. Drouin, A.R. Couture, D. Joly, X. Tastet, V. Aimez, and R. Gauvin, "CASINO V2.42—A Fast and Easy-to-use Modeling Tool for Scanning Electron Microscopy and Microanalysis Users," Scanning **29**(3), 92–101 (2007).
[55] S. Boughaleb, B. Martin, C. Matei, R. Templier, Ł. Borowik, N. Rochat, B. Gil, and A. Dussaigne, "Selective area growth of AlGaN nanopyramids by conventional and pulsed MOVPE," Nanotechnology **32**(19), 195203 (2021).
[56] V. Jindal, J. Grandusky, F. Shahedipour-Sandvik, S. LeBoeuf, J. Balch, and T. Tolliver, "Selective Area Heteroepitaxy of Nano-AlGaN UV Excitation Sources for Biofluorescence Application," MRS Proc. **916**, 0916-DD05-03 (2006).
[57] S.C. Cruz, S. Keller, T.E. Mates, U.K. Mishra, and S.P. DenBaars, "Crystallographic orientation dependence of dopant and impurity incorporation in GaN films grown by metalorganic chemical vapor deposition," J. Cryst. Growth **311**(15), 3817–3823 (2009).